Supporting Information

Embedded 3D printing of Multi-material composites

Shitong Zhou [a,], Iuliia S Tirichenko [a], Xun Zhang [b], Yinglun Hong [a], Harry Payne [a], Philip Withers [b], Florian Bouville [a], Eduardo Saiz [a,]**

[a] Centre of Advanced Structural Ceramics, Department of Materials, Imperial College London, London, SW7 2AZ, UK. Email: s.zhou18@imperial.ac.uk, e.saiz@imperial.ac.uk

[b] Henry Royce Institute, Department of Materials, The University of Manchester, Manchester, M13 9PL, UK

Table S1 Rheological behavior of ink and matrix suspensions

Pluronic (wt%)	Solid loading (vol%)	T (°C)	σ_y^{Stat} (Pa)	σ_y^{Dyn} (Pa)	G'_{eq} (Pa)	Flow point (Pa)	n	K (Pa·s^n)	$\tau_{y,min}$ (Pa)	h_{min} (mm)
25	Steel 25	15	1.11	0.86	N/A				2.13	N/A
		16	2.92	1.13	1.4×10^4	242	0.14	248		
		17	295.01	121.23	1.9×10^4	353	0.20	406		
		25	739.00	442.36	3.9×10^4	677	0.26	268		
25	Steel 30	15	3.16	1.66	N/A				2.92	
		16	10.70	1.96	1.8×10^4	274	0.21	270		
		17	236.29	172.60	2.3×10^4	388	0.25	276		
		25	743.65	442.09	4.9×10^4	700	0.27	297		
30	Steel 30	15	693.63	454.17	2.8×10^4	542	0.25	287	2.92	
		16	794.74	485.06	3.0×10^4	585	0.23	313		
		17	801.86	520.66	3.3×10^4	652	0.26	334		
		25	791.43	690.49	4.4×10^4	748	0.25	463		
30	Steel 35	15	812.91	415.85	3.5×10^4	585	0.26	437	3.98	
		16	818.67	464.06	3.3×10^4	607	0.19	730		
		17	770.90	453.68	3.6×10^4	641	0.19	730		
		25	913.16	637.16	5.2×10^4	796	0.22	779		
30	Steel 40	15	816.48	336.85	5.4×10^4	610	0.17	1455	5.04	
		16	869.94	371.72	5.3×10^4	623	0.30	858		

		17	1020.68	420.33	5.2×10^4	655	0.19	1114		
		25	1133.63	603.73	7.8×10^5	737	0.21	1768		
		10	179.78	15.87						
		11	241.08	18.48	N/A					
		12	246.54	38.59						
		13	367.89	166.07	3.0×10^4	181	0.47	1417		
30	Graphite 25	14	541.18	248.64	4.0×10^4	238	0.33	1910	2.69	
		15	640.52	290.04	4.8×10^4	281	0.32	2056		
		16	701.37	426.68	5.6×10^4	291	0.30	2252		
		17	836.81	415.64	6.2×10^4	320	0.30	2489		
		25	974.01	836.42	1.4×10^5	511	0.27	2483		
		10	26.25	2.12	0.8×10^2	6.4	0.53	12		0.1
		11	19.90	2.43	0.9×10^2	5.8	0.41	19		0.1
		12	22.95	2.82	1.0×10^2	5.0	0.45	23		0.1
		13	12.17	2.58	1.8×10^2	5.7	0.46	27		0.1
25	Al_2O_3 37	14	8.69	3.81	2.8×10^2	6.1	0.60	24	N/A	0.2
		15	9.50	12.03	0.13×10^4	23	0.83	18		0.6
		16	69.67	74.01	0.67×10^4	186	0.89	22		3.6
		17	306.08	258.46	1.0×10^4	290	0.35	279		12.5
		25	1143.66	897.10	2.4×10^4	503	0.19	946		43.4

Table S2 Density, thermal expansion, plasticity, elastic modulus and poisson's ratio of steel and Al_2O_3 used for finite element modelling[1,2]

Material	Density (kg/mm^3)	Thermal Expansion (/°C)	Plastic			Elastic modulus (MPa)	Poisson's ratio
			Temperature (K)	Yield stress (MPa)	Plastic strain (%)		
Fiber: steel	7.7e-6	12e-6	300	400	0	200e3	0.29
				500	0.1		
			700	280	0		
				320	0.1		
			900	50	0		
				55	0.1		
			1400	10	0	100e3	0.36
				11	0.1		
Matrix: Al_2O_3	3.97e-6	8e-6	300			370e3	0.24
			700			360e3	0.24
			1100			350e3	0.26
			1300			340e3	0.31

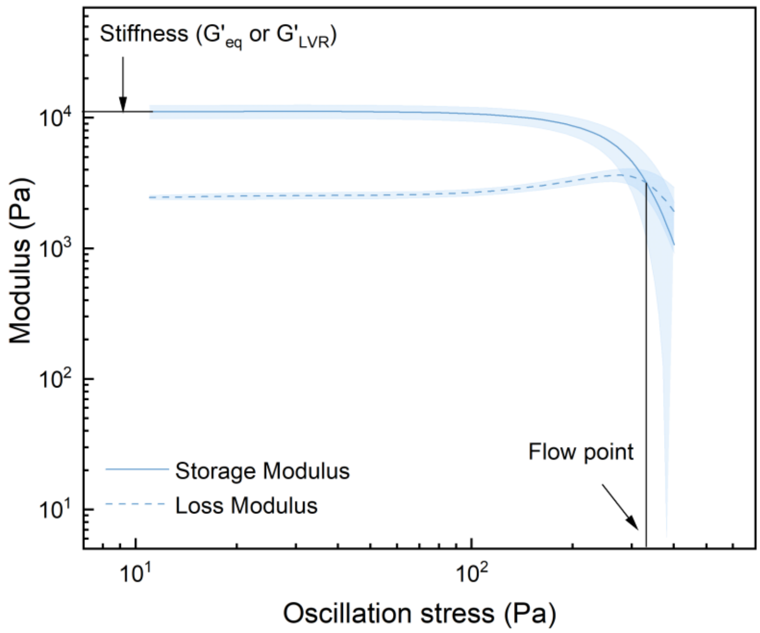

Figure S1. Dynamic mechanical analysis was performed to determine the viscoelastic properties of matrix over the liquid-gel transition temperature range and at room temperature, with illustration at 17°C. Under low stress, the matrix behaves viscoelastic and solid-like behavior. Storage modulus G' is almost constant and higher than loss modulus G". The storage modulus at low stress is regarded as stiffness of matrix, also denoted as the storage modulus in linear viscoelastic region G'_{LVR} or equilibrium storage modulus, G'_{eq}. The gel network breaks down as the stress increases, resulting in a gradual decrease of G' and the beginning of an increase in G". When G' is equal to the G", the matrix starts to flow, and the stress at this point is called flow point, also termed yield stress.

Packing limit of inks

The situation of ink with inorganic powder is similar to a ceramic injection molding system[3], where the viscosity can be fitted to the Krieger-Dougherty model[4]:

$$\frac{\eta_0}{\eta_{0,Pluronic}} = (1 - \frac{\varphi}{\varphi_m})^{-[\eta]\varphi_m} \quad \text{Eq 1}$$

where η_0 is viscosity of paste at zero shear rate, $\eta_{0,Pluronic}$ is the viscosity of the continuous medium, here the Pluronic gel, φ is volume fraction or solid loading, φ_m is the packing fraction (theoretical maximum solid loading, at which the viscosity becomes infinite) and $[\eta]$ is the intrinsic viscosity, reported to be 2.5 for hard uniform spheres.[4] At 17 ℃, the packing limit of steel in 30wt% Pluronic gel is calculated to be 0.45 (Fig. S2). Sintered composites fabricated with ink formulations of 30wt% Pluronic 40vol% steel, close to the packing limit, are found to have a steel filament cross-sectional area apparently smaller than as-designed compared with other ink compositions (Fig. 2e_{iii}). This small filament is accompanied by a low interlayer and intralayer resolution when building dense structures, suggesting this ink is not suitable for printing.

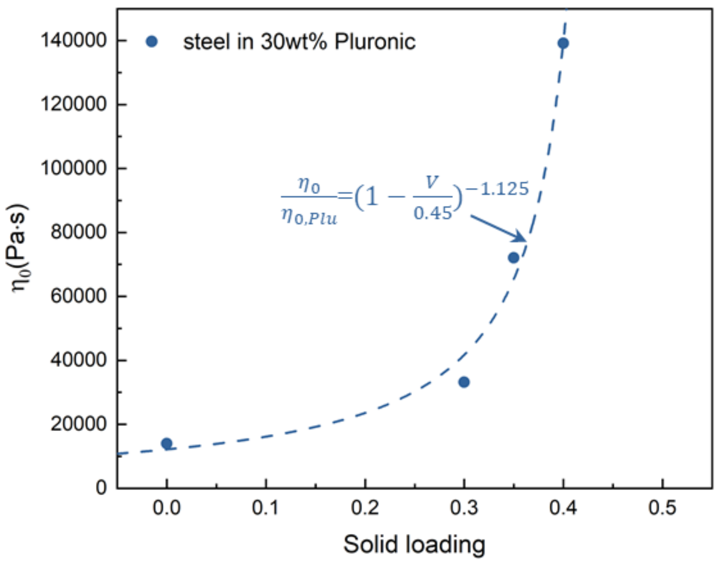

Figure S2. The effect of solid loading on viscosity at zero shear rate, fitted with Krieger-Dougherty model

Plateau-Rayleigh instability

This instability is attributed to interfacial tension between ink and matrix $\gamma_{ink-matrix}$ and limits the filament diameter. At a diameter smaller than the minimum stable size, $\frac{\gamma_{ink-matrix}}{\tau_y}$, droplets form when printing a liquid ink with zero yield stress in a fluid with a τ_y>0.[5] In this work, both ink and matrix are based on Pluronic gels with inorganic powders so $\gamma_{ink-matrix}$ should be small. Since ink and matrix are Herschel Bulkley fluids, τ_y is supposed to be the difference of yield stress between ink and matrix. As such, it is reasonable to choose an ink with higher yield stress than the matrix to minimize the stable diameter and avoid droplet formation. The diameter of graphite and steel filaments (Fig. 1e-h) is relatively large and therefore they do not break intro droplets.

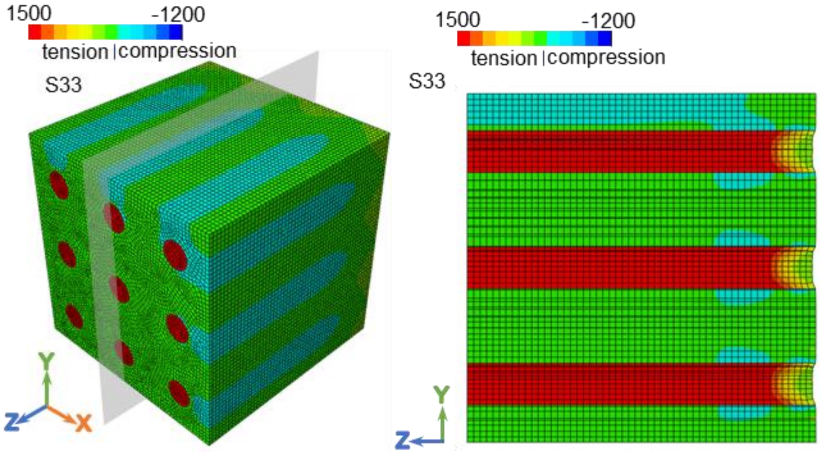

Figure S3. FEM of thermal stress in fiber arrays reinforced alumina

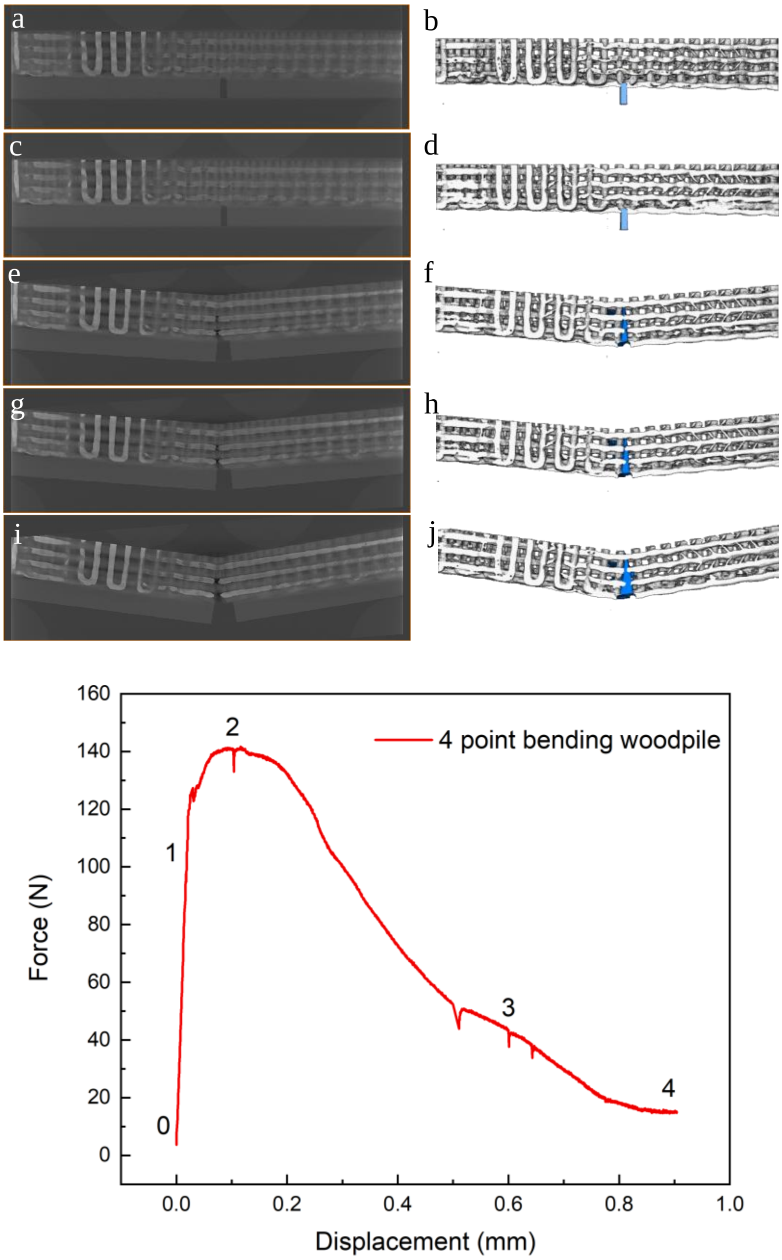

Figure S4. X-ray CT of steel woodpile reinforced Al_2O_3 (2D virtual slice through middle of beam and 3D rendering with the ceramic matrix (rendered transparent), steel (grey), notch (light blue) and crack (blue) during 4-point bending at step 0(a-b), step 1(c-d), step 2(e-f), step 3(g-h), step 4(i-j) and the corresponding force-displacement curve

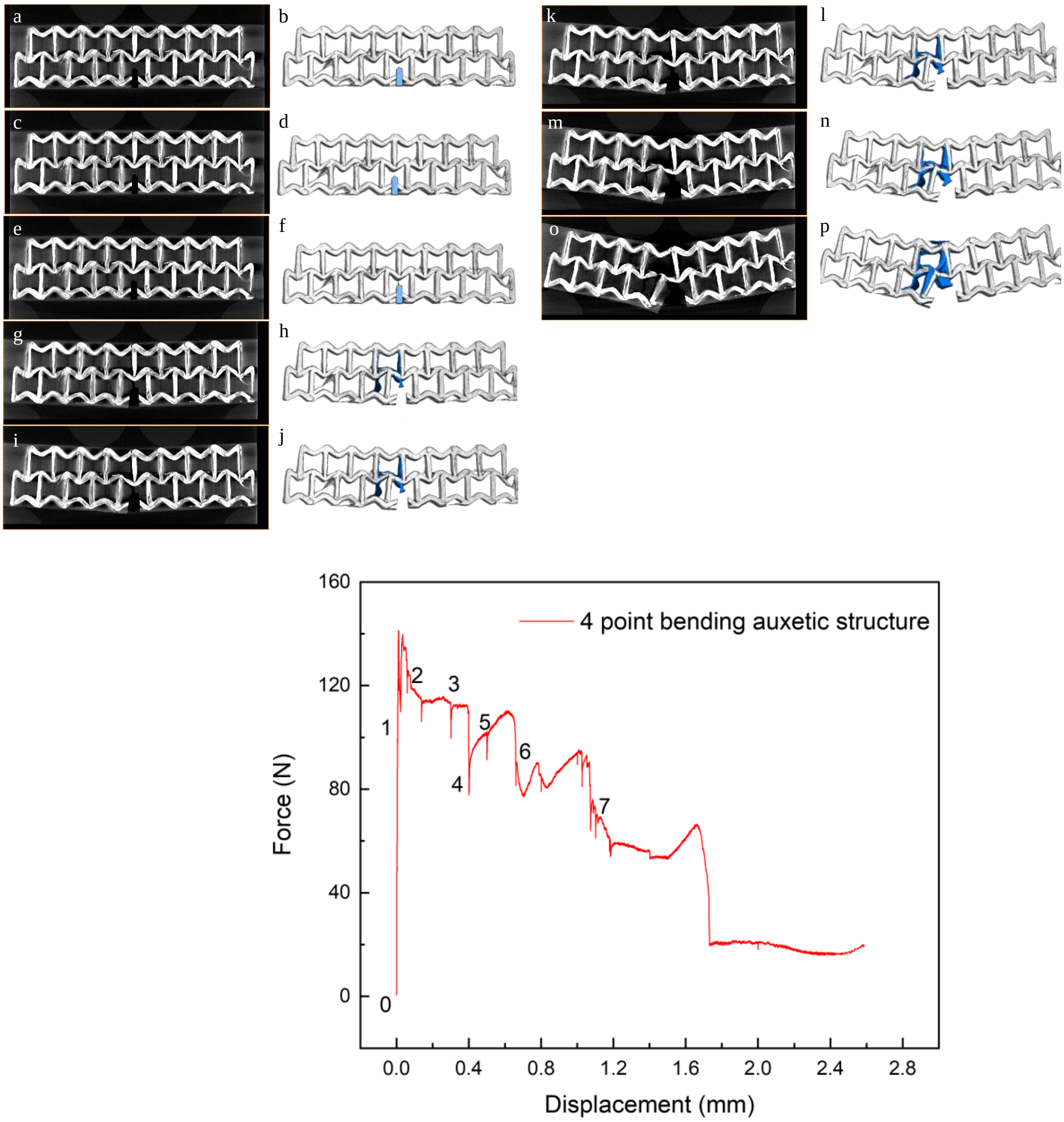

Figure S5. X-ray CT of steel auxetic reinforced Al_2O_3 (2D virtual slice through middle of beam and 3D rendering with the ceramic matrix (rendered transparent), steel (grey), notch (light blue) and crack (blue) during 4-point bending at step 0(a-b), step 1(c-d), step 2(e-f), step 3(g-h), step 4(i-j), step 5(k-l), step 6(m-n), step 7(o-p) and the corresponding force-displacement curve

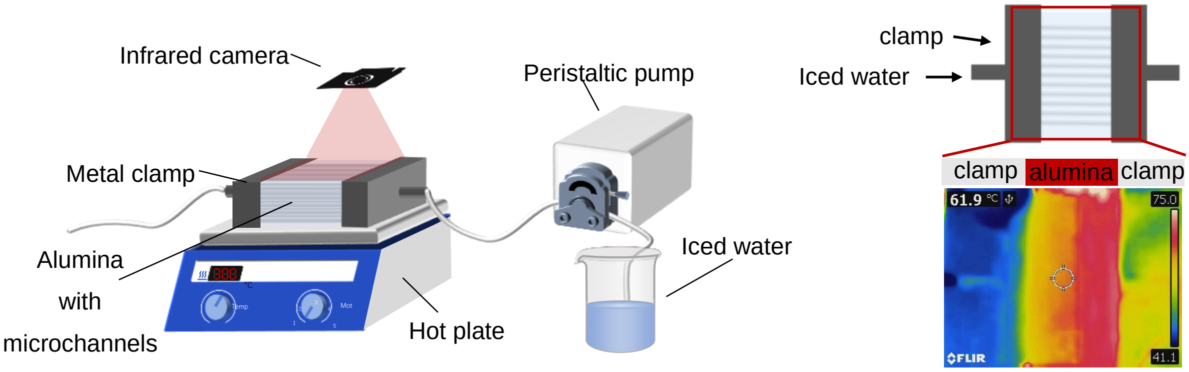

Figure S6. Setup for testing the connectivity of the microchannels

References

1 Auerkari, P. *Mechanical and physical properties of engineering alumina ceramics*. Vol. 23 (Technical Research Centre of Finland Espoo, 1996).

2 Fukuhara, M. & Sanpei, A. Elastic moduli and internal friction of low carbon and stainless steels as a function of temperature. *ISIJ international* **33**, 508-512 (1993).

3 Edirisinghe, M. J., Shaw, H. M. & Tomkins, K. L. Flow behaviour of ceramic injection moulding suspensions. *Ceramics International* **18**, 193-200, doi:https://doi.org/10.1016/0272-8842(92)90095-U (1992).

4 Krieger, I. M. & Dougherty, T. J. A Mechanism for Non-Newtonian Flow in Suspensions of Rigid Spheres. *Transactions of the Society of Rheology* **3**, 137-152, doi:10.1122/1.548848 (1959).

5 Mahmoudi, M., Burlison, S. R., Moreno, S. & Minary-Jolandan, M. Additive-Free and Support-Free 3D Printing of Thermosetting Polymers with Isotropic Mechanical Properties. *ACS Appl Mater Interfaces* **13**, 5529-5538, doi:10.1021/acsami.0c19608 (2021).